RESEARCH ARTICLE

Macromolecular Rapid Communications
www.mrc-journal.de

Atomistic Molecular Dynamics Simulations of ABA-Type Polymer Peptide Conjugates: Insights into Supramolecular Structures and their Circular Dichroism Spectra

Moritz L. Obenauer, Johannes A. Dresel, Maren Schweitzer, Pol Besenius, and Friederike Schmid**

A combination of atomistic molecular dynamics (aMD) simulations and circular dichroism (CD) analysis is used to explore supramolecular structures of amphiphilic ABA-type triblock polymer peptide conjugates (PPC). Using the example of a recently introduced PPC with pH- and temperature responsive self-assembling behavior [Otter et al., Macromolecular Rapid Communications 2018, 39, 1800459], this study shows how molecular dynamics simulations of simplified fragment molecules can add crucial information to CD data, which helps to correctly identify the self-assembled structures and monitor the folding/unfolding pathways of the molecules. The findings offer insights into the nature of structural transitions induced by external stimuli, thus contributing to the understanding of the connection of microscopic structures with macroscopic properties.

1. Introduction

Polymer peptide conjugates are a modern class of hybrid materials that synergistically combine the favorable properties of synthetic polymers and polypeptides.[1,2] The advantages and limitations of synthetic polymers are well-known: Their production is inexpensive, but possibilities to modify individual monomers or control the molecular weight distribution are limited.[3] In contrast, biological and synthetically accessible polypeptides via solid phase peptide synthesis (SPPS), consisting of amino acids linked by peptide bonds, are monodisperse and their sequences can be designed.[4] In solution, they form highly ordered and stable superstructures based on supramolecular interactions, which makes them attractive as carriers and biologically active materials. Linking these biopolymers to synthetic polymers such as polyethylene oxide (PEO) increases their stability and can improve their pharmaceutical efficacy.[5]

Important questions about structure-property relationships of these materials are difficult to answer in laboratory experiments. These include, for example, the secondary structure of polypeptides, the influence of polymer chain length, and pathways of self-assembly.[6,7] Computational chemistry can contribute to answering these questions: Atomistic molecular dynamics simulations (aMD) are necessary to reproduce details such as the secondary structure and folding of polypeptides, whereas coarse-grained simulations, that require much less computational time, are often sufficient to describe polymer chains.[8] Computational studies and simulations of PEGylated proteins have become a standard technique in theoretical chemistry.[9,10] The influence of polyethylene oxide (PEO) on helix stability of polypeptides has been an active area of research.[11–13] However, more advanced designs such as ABA-type triblock polymer peptide conjugates with two polypeptide moieties (A) and one PEO unit (B) have not yet been covered sufficiently.[8]

The secondary structure and folding events of polypeptides and proteins can be analyzed and studied with circular dichroism (CD) spectroscopy. Secondary structures introduce an additional dimension of order and chirality to the molecule and molecular arrangement, giving rise to different absorption coefficients for right-handed and left-handed circular polarized light.[14,15] Classical computer-aided or machine-learning-based approaches for analyzing and deconvoluting complex CD spectra are available for extended systems for polypeptides or proteins.[16–18] These mathematical decomposition algorithms are less suited for smaller oligopeptides since only a few amino acids contribute to the CD spectrum. Alternatively, one can predict CD spectra from quantum mechanical (QM) calculations.[19,20] Unfortunately, these calculations need the folded geometry of the given system as an input, since QM-based geometry optimizations on the scale of solvated proteins are practically not feasable. In the present work, we propose, as an alternative

M. L. Obenauer, J. A. Dresel, M. Schweitzer, P. Besenius
Department of Chemistry
Duesbergweg 10-14, D-55128 Mainz, Germany
E-mail: besenius@uni-mainz.de
F. Schmid
Institute of Physics
Staudingerweg 7-9, D-55128 Mainz, Germany
E-mail: friederike.schmid@uni-mainz.de

The ORCID identification number(s) for the author(s) of this article can be found under https://doi.org/10.1002/marc.202400149

DOI: 10.1002/marc.202400149

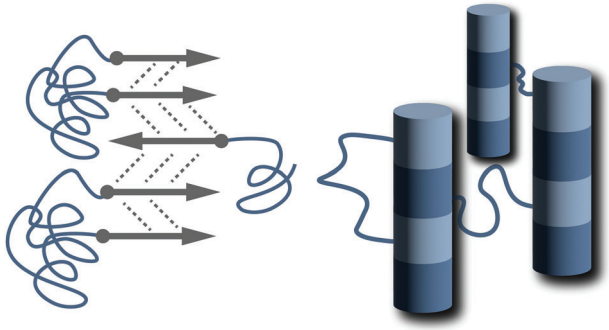

Figure 1. Proposed aggregation mechanism of linear polymer peptide conjugates. The polypeptide moieties form stable β-sheet structures (left) and connect the different molecules to form supramolecular 1D nanorods in solution (right). These nanorods lead to a network formation and a self-supporting hydrogel, as previously reported.[21] Different shades of blue are used to visualize different molecules of the same type.

approach, to combine CD measurements with aMD simulations. We will demonstrate how simulation results can help to discriminate between possible interpretations of CD signals, and how they can give additional information on molecular structure.

As a model system to demonstrate the approach, we choose a subclass of ABA-type polymer peptide conjugates, which has recently been introduced by Otter et al., where both oligopeptides (A) are attached to the polyethylene oxide (PEO) block (B) via the C-terminus.[21] These C_2 symmetric molecules with hydrophobic FHFHF (F: L-Phenylalanine, H: L-Histidine) sequences showed supramolecular self-assembly and changing hydrogel characteristics depending on the pH value (**Figure 1**). Polymer peptide conjugates are known to be temperature-sensitive, which is proposed to be caused by the lower critical solution temperature (LCST) behavior of PEO, while the basic imidazole side chains of the histidine residues account for the pH responsiveness.[22] The pathway of supramolecular self-assembly and the aggregation mechanism for Otter ABA-type systems have not yet been studied computationally. The underlying structural transitions upon changing the pH value were estimated by circular dichroism spectroscopy. However, applying deconvolution methods to analyze the CD spectra is challenging, since only ten amino acids contribute to the CD signal.

In the present work, we will demonstrate how a combination of aMD simulations and CD measurements can be used to identify possible secondary structures of this specific ABA tribock system, and, in particular the structure that is predominant in solution. In addition, we study unfolding pathways upon changing pH or raising the temperature. We use aMD simulations on the microsecond timescale to calculate these structures under different conditions and validate our findings with circular dichroism spectroscopy. More generally, we propose a methodology to treat artificial polymer peptide conjugates computationally, which can lead to a better understanding of folding and unfolding processes of oligopeptides. This therefore lays a foundation for the understanding of biological activities of these artificial biomolecules in solution and viscoelastic properties of gels in the semi-dilute regime.

2. Methods

2.1. Computational Modeling

Instead of simulating the polymer peptide conjugates Ac-FHFHXG-PEO$_n$-GXFHFHF-Ac (**PPC**) directly, we studied the fragment molecule Ac-FHFHXG-OH (**Pep**). The chemical structure and the corresponding model are shown in **Figure 2**. Using the fragment system instead of the actual polymer peptide conjugate speeds up the computations by one order of magnitude, even considering that the costs of the full simulation can be reduced by modeling the PEO repeat units only at the united-atom level. Our simplification rests on the assumption that the telechelic polypeptides should behave independently of one another if the connecting PEO chains are sufficiently long: Aggregation processes are governed by diffusion rather than spatial proximity caused by the connecting PEO chains. Perturbations of the secondary structure due to the PEO chain are assumed to be small, and their study is beyond the scope of this research.

In the simulations, we use the OPLS-AA/M force field with the TIP4P water model, since this combination proved to give polypeptide secondary structures that are in very good agreement with quantum mechanical calculations.[23–31] To simulate laboratory conditions and neutralize any charges that might occur, the sodium chloride concentration was set to 10 mmol L^{-1}. Force field parameters for all standard amino acids in neutral and charged variants are available in atomistic resolution in the OPLS-AA/M force field. However, 6-aminohexanoic acid (X) is a bifunctional C6-spacer in the polypeptide chain and had not yet been parameterized prior to the present work. We mapped in united-atom resolution following established procedures; see Supporting Information for details.[32–36] The starting geometries were generated using the software Project RACCOON.[37]

2.2. Simulation Techniques and Trajectory Analysis

Simulations were performed using standard GROMACS input parameters for atomistic force fields.[38] First, the steepest descent algorithm performed an energy minimization of 200 kJ mol^{-1} nm^{-1}. After initial energy minimization, velocities were generated at the specified temperature according to the Maxwell-Boltzmann distribution, and the temperature was equilibrated by the V-Rescale thermostat for 100 ps.[39] For this and all subsequent simulation runs, both Coulomb and van der Waals forces were truncated after 1 nm, with the long-range components of the electrostatic potentials calculated using the fast smooth Particle-Mesh Ewald method.[40] To compensate for artifacts of the truncated van der Waals potentials, the dispersion correction for energy and pressure was used.[41,42] The atoms of the simulated molecules were coupled independently of the water molecules in two different temperature baths, each with a time constant of 0.1 ps. Subsequently, the pressure was equilibrated for 100 ps using the isotropic Parrinello-Rahman pressure coupling.[43] The pressure was fixed at 1 bar with a time constant of 2 ps and a compressibility of 0.045 mbar. After the successful equilibration steps, the production run was performed for 1 µs at appropriate temperatures using the leapfrog integrator with a time step of 2 fs. The LINCS algorithm fixed all bonds between hydrogen atoms and heavier atoms.[44] All simulations were

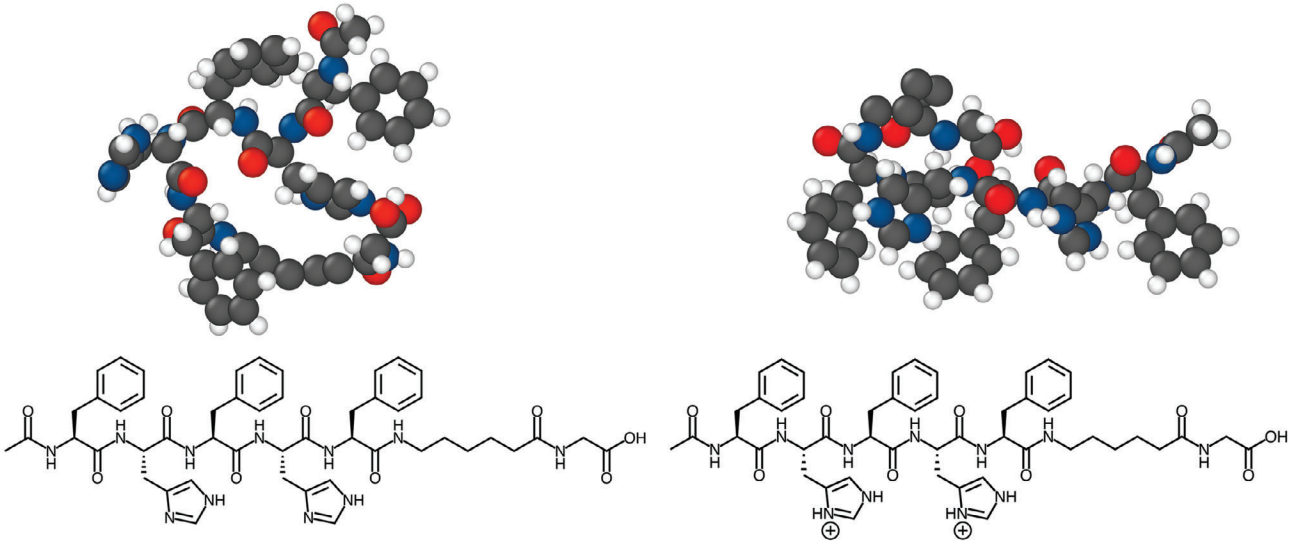

Figure 2. Chemical structure of **Pep** (left). The molecular model used in this study is shown above. Chemical structure of $\mathbf{Pep}^{2+}$ (right). The molecular model for $\mathbf{Pep}^{2+}$ with two additional hydrogen atoms at the histidine residues is shown above the structure. **Pep** and $\mathbf{Pep}^{2+}$ are modeled in full atomistic detail except for six-amino hexanoic acid (X), where carbon and hydrogen atoms are contracted following the united-atom approach. The C-terminus is always protonated in this study since the polymer peptide conjugate **PPC** has no free carboxylic acid groups. Color coding: Carbon: dark gray, Hydrogen: light gray, Oxygen: red, Nitrogen: blue.

performed with periodic boundary conditions with a dodecahedral box size of 5.8 and 7.0 nm for the single chains and dual chains, respectively. The dodecahedral simulation box was chosen for its smaller volume compared to a cubic simulation box and therefore save on computational costs. Energies and positions of atoms were stored every 5000 steps (10 ps). All aMD simulations were performed with the GROMACS 2022.5 software package.[45]

The obtained trajectories were modified with *gmx trjconv* so that only the atoms of the polypeptides were retained. The coordinates of the water molecules and ions were not used for the following analyses. Analysis was performed using *mdanalysis* and *Python*-based in-house scripts.[46–48] Contracted Ramachandran plots (CRP) are used here to compare the dihedral angle distributions across different simulation runs. CRPs reduce the 2D density function obtained from a Ramachandran analysis to a 1D normalized density distribution by integrating over one of the two dihedral angles Φ or Ψ (see Supporting Information for more information). Ramachandran space nomenclature as introduced by Hollingsworth and Karplus in 2010 is used.[49]

2.3. Experimental Section

The peptide sequence Ac-FHFHFXG-OH was synthesized via solid phase peptide synthesis on 2-chlorotrityl resin using standard Fmoc-protocols.[50] To preserve the trityl protection groups on the histidine sidechains for the next synthesis step, cleavage from the resin was performed with trifluoroethanol.[21] After PyBOP-mediated coupling of the peptide sequence to aminodifunctionalized PEO (M_w: 3000 g mol^{-1}), trityl groups were removed using trifluoro acetic acid. The crude product was purified via size exclusion chromatography. The resulting Ac-FHFHFXG-PEO_n-GXFHFHF-Ac was characterized by ^{1}H-NMR and MALDI-ToF (see Supporting Information for further information).

The samples for circular dichroism spectroscopy were prepared by dissolving Ac-FHFHFXG-PEO_n-GXFHFHF-Ac in 10 µM phosphate buffer solution (pH 7.77) and filtering it through a syringe filter. CD spectra were recorded on a J-815 CD spectrometer from JASCO (Pfungstadt, Germany) using the software Spectra Manager 2.08.04. All samples were measured three times each to obtain accumulated spectra. Spectra were recorded between 190 nm and 300 nm if not stated otherwise. Samples had a concentration of 50 µM in phosphate buffer solution.

3. Results and Discussion

3.1. Single Chain Simulations of Ac-FHFHFXG-OH

To obtain a reference of how a single, non-interacting Ac-FHFHFXG-OH (**Pep**) sequence behaves in solution, a single molecule was first simulated at 300 K. Two maxima are found in the Ramachandran plot at $\Phi, \Psi = (-80°, 140°)$ and $\Phi, \Psi = (-150°, 155°)$ (**Figure 3**, left). The maximum at $\Phi, \Psi = (-80°, 140°)$ (Polypeptide II, P_{II}) is the dominant structural feature. This main maximum indicates that the short polypeptide sequence adopts the P_{II} conformation to maximize chain entropy while enhancing the accessibility of hydrogen bonds to the surrounding water molecules.[51] Furthermore, this chain conformation perturbs the organization of the water molecules as little as possible. The P_{II} region had been overlooked at the beginning of conformational analyses of proteins and polypeptides and was seen as a subgroup of the β-sheet region adopted only by polyproline. Recent studies proved that the P_{II} structures are a common motif in all polypeptides.[52] Even though this structure is mainly observed for unfolded polypeptides, it is still an ordered linear secondary structure and not a random chain conformation.[49] Thus, in what follows, a dominant maximum at $\Phi, \Psi = (-80°, 140°)$ is assumed to be the native, unfolded P_{II} conformation of the

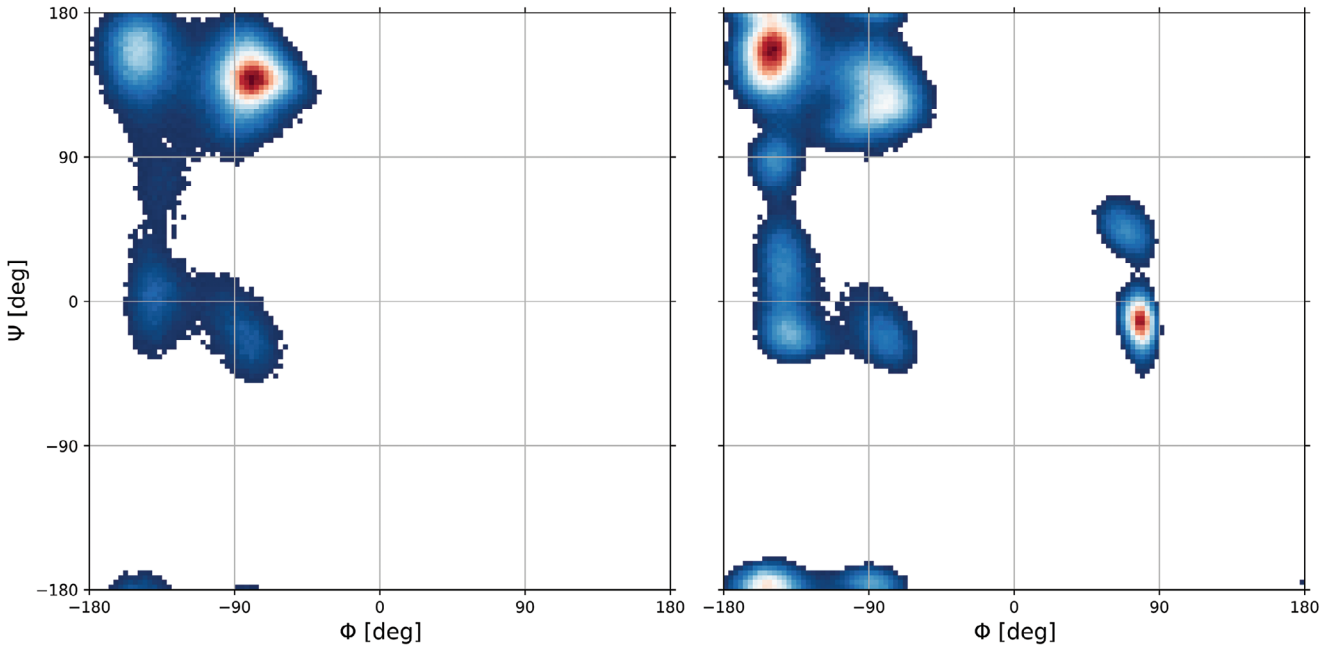

Figure 3. Ramachandran plots of **Pep** (left) and the dimer $(\mathbf{Pep})_2$ (right.) The single chain shows a maximum in the P_{II} region ($\Phi, \Psi = (-80°, 140°)$) with a secondary maximum in the β-sheet region ($\Phi, \Psi = (-150°, 155°)$). Two aggregated chains (right) exhibit major maxima in the β-sheet ($\Phi, \Psi = (-150°, 155°)$) and δ' region ($\Phi, \Psi = (80°, -10°)$). For better visibility, data points with a relative frequency lower than 10^{-5} are omitted.

polypeptides. The existence of the significantly less intense secondary maximum at $\Phi, \Psi = (-150°, 155°)$ proves that the single chain can also adapt a conformation resembling a β-sheet. However, this conformation is three times less frequent than the P_{II} structure.

To further investigate the behavior of the single chain conformations, the **Pep** sequence was additionally simulated at higher temperatures, up to 330 K, in steps of 10 K. The adapted conformation is very sensitive to temperature changes. Increasing the temperature from 300 to 330 K leads to a relative decrease in the P_{II} structure while conformations with $\Phi, \Psi = (-150°, -20°)$ become more populated. This is a non-linear effect and the maximum at $\Phi, \Psi = (-150°, -20°)$ is most pronounced for the simulation at 310 K compared to even higher temperatures. However, since this effect is subtle and the dominant structural feature P_{II} is still present, we interpret these results not as a transition to another distinct conformation but as an undefined increase of α-helix structural features upon heating.[49] These differences in backbone angles at different temperatures are depicted in **Figure 4**. These results indicate that the temperature dependence of Otter's polymer peptide conjugates might not be only attributed to the LCST behavior of PEO but can be influenced

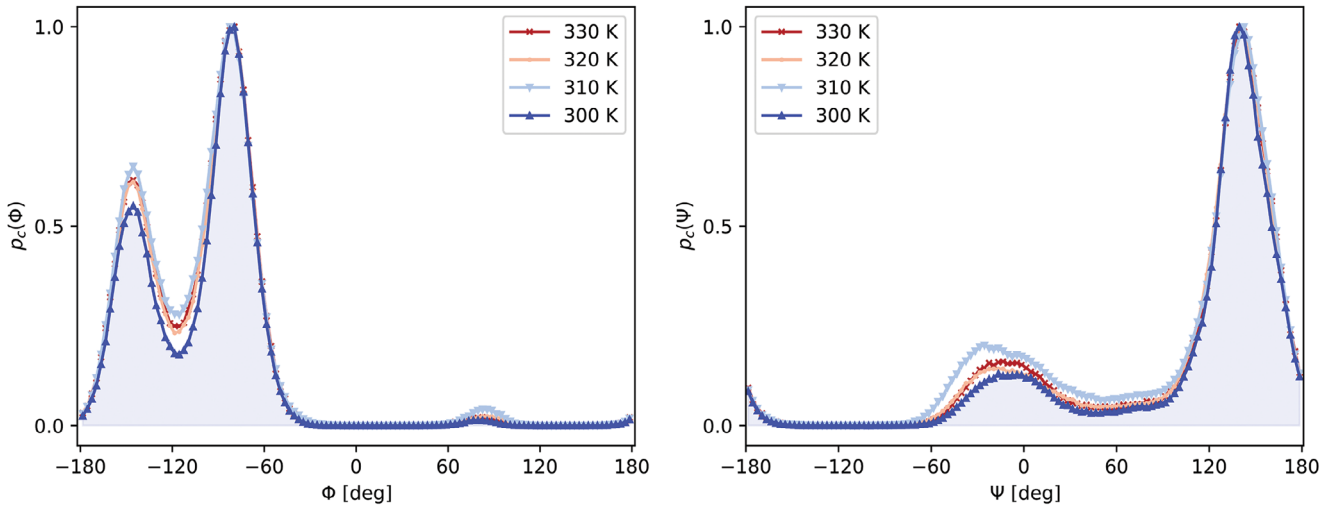

Figure 4. Contracted Ramachandran plots of **Pep** at different temperatures. Upon heating the probability of α-helix like structures at $\Psi = (-20°)$ increases. The major structural feature is P_{II} independent of the temperature. We interpret these results not as a transition to another distinct conformation but as an undefined increase of α-helix structural features upon heating.[49]

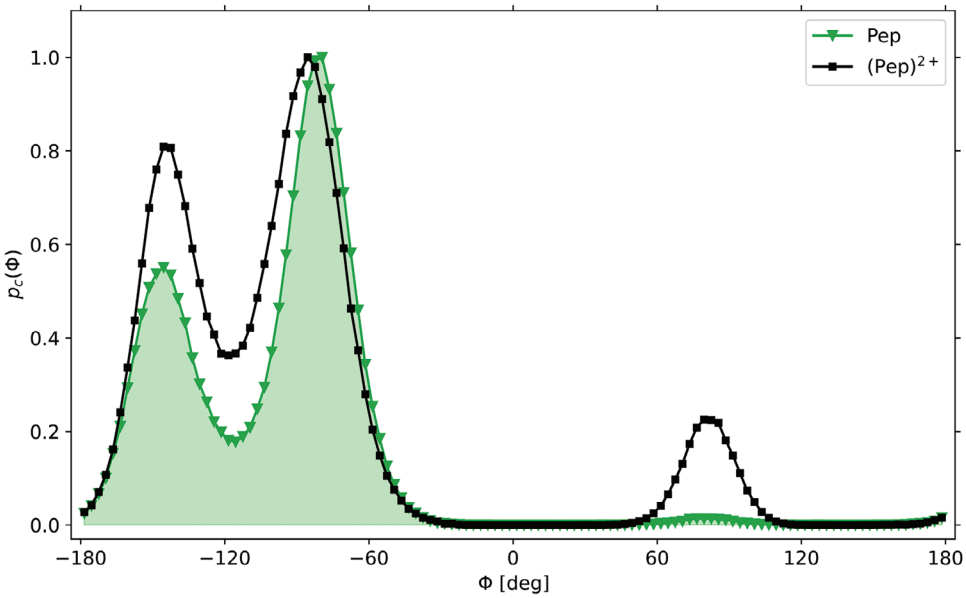

Figure 5. Contracted Ramachandran plots of **Pep** (green) and $(\mathbf{Pep})^{2+}$ (black). Both in the neutral and charged state, the P_{II} ($\Phi = (-80°)$) is the dominant structural feature. Upon full protonation, the probability $p_c(\Phi)$ of the β-sheet ($\Phi = (-150°)$) and δ' ($\Phi = (80°)$) regions increase. The increased electrostatic repulsion between the charged imidazolium side chains leads to this change in conformation.

by the temperature dependence of the polypeptide moieties of the molecule.

The protonated single chain $(\text{Ac-FHFHFXG-OH})^{2+}$ ($(\mathbf{Pep})^{2+}$) was simulated and analyzed like its neutral counterpart at 300 K. In the charged state, the chain shows structural features with an angle $\Phi = (80°)$, which are not present in the neutral state (**Figure 5**). Furthermore, the probability of adopting conformations with $\Phi = (-150°)$ increases to $p_c(\Phi) = 0.8$, indicating a straightened structure compared to the neutral molecule. These changes in geometry account for the increased electrostatic repulsion between the positively charged imidazolium side chains of the histidine moieties (see Supporting Information for further information).

3.2. Two-Chain Simulations of Ac-FHFHFXG-OH Dimers

Two **Pep** molecules were simulated in one simulation box to mimic the behavior of the two polypeptide moieties of **PPC** for long PEO polymer chains. In a neutral state the two chains form stable aggregates (Ac-FHFHFXG-OH dimers, $(\mathbf{Pep})_2$) with anti-parallel alignment over the trajectory time of 1 µs. This stable aggregation can be characterized by the radius of gyration $R_G = (7.6 \pm 0.3)$ Å (see Supporting Information) and the distance between the two chains $R_{AB} = (6.2 \pm 1.0)$ Å (see Supporting Information). This anti-parallel alignment seems to be thermodynamically favored and not a kinetically trapped state, since the initial geometry of the two chains was chosen to be parallel.

To further characterize the secondary structure, a Ramachandran analysis was performed, which is shown in Figure 3 (right). Three distinct regions can be observed with a major maximum in the β-sheet region $\Phi, \Psi = (-150°, 155°)$ indicating the formation of anti-parallel β-sheets between the two chains. However, this structure is not fully linear, but exhibits a type II β-turn, which is derived from the existence of the secondary maximum in the δ' region ($\Phi, \Psi = (80°, -10°)$) only occupied by one histidine residue.[49] The minor maximum at $\Phi, \Psi = (-80°, 120°)$ resembles the already described P_{II} structure and can be interpreted as corresponding to two chains in a non-aggregated state. This is expected due to thermal fluctuations and the initial lag time before the two chains form a stable aggregate. Even though there are two major maxima in the Ramachandran space (β and δ'), they both describe one single secondary structure and not two dynamically interchanging distinct conformations (see Supporting Information for further information).

In addition, the charged system with two fully protonated histidine units per chain was simulated for 1 µs at 300 K. Instead of forming a stable Ac-FHFHFXG-OH dimer, dynamic folding, and unfolding processes of the two chains are observed. The R_G and R_{AB} fluctuate periodically (see Supporting Information), indicating dynamic association and dissociation behavior. Even in an associated state the chain distance never falls below 10 Å, implying a less stable structure caused by the higher electrostatic forces between the charged side chains compared to the neutral state (see Supporting Information). Contact maps for Ac-FHFHFXG-OH dimers and two protonated $(\text{Ac-FHFHFXG-OH})^{2+}$ chains were created (**Figure 6**). An *x-pattern*, which is characteristic for anti-parallel β-sheets, is apparent in the neutral state. However, the first and third quadrants of the contact map for the charged state show increased intermolecular distances, further proving the dissociated and unfolded state upon full protonation.

The Ramachandran analysis shows a broad distribution in the P_{II} region, resembling the $(\mathbf{Pep})^{2+}$ distribution and hence indicating that a significant amount of chains in the charged state are unfolded (**Figure 7**). The protonation gives rise to a higher population of the δ' and ϵ regions, further hinting at a structural change upon full protonation. Based on these results, we propose a β-sheet → P_{II} unfolding pathway after the protonation of the

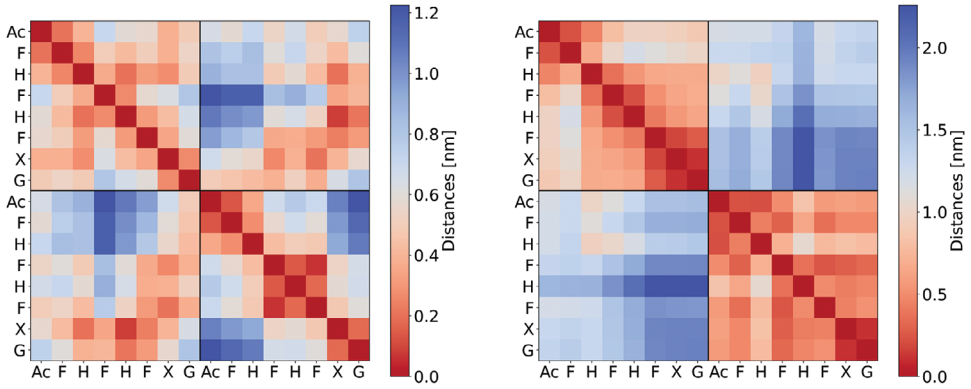

Figure 6. Spatial proximity contact maps for Ac-FHFHFXG-OH dimers $(\mathbf{Pep})_2$ (left) and the protonated system $(\mathbf{Pep})_2^{4+}$ (right). Distances are given in nm. In the aggregated state of $(\mathbf{Pep})_2$ the characteristic *x-pattern* for anti-parallel β-sheets is observed. In the protonated state, the two chains do not form a stable aggregate and show increased intramolecular distances.

histidine side chains. It is important to note that in the charged state, none of the simulations indicate that the polypeptides adopt a random conformation.

These findings agree with the experimental results that at low pH values (full protonation of the imidazole side groups) the **PPC** hydrogels at $w = 1.5\%$ are no longer self-supporting.[21] The lack of aggregation on the molecular level leads to suppressed network formation on the microscale and, therefore, no hydrogel formation on the macroscale.

3.3. Circular Dichroism Spectra of Ac-FHFHFXG-PEO$_n$-GXFHFHF-Ac

Electronic circular dichroism (CD) spectra for the **PPC** polymer peptide conjugates were recorded at varying pH values (**Figure 8**) and temperatures (**Figure 9**). In accordance with previous results, two distinct signals independent of temperature and pH value ($\lambda = 205$ nm: negative band, $\lambda = 220$ nm: positive band) are observed in the CD spectrum.[21] Since the positive band at $\lambda = 220$ nm decreases sigmoidally upon protonation of the histidine side chains, this signal intensity was used previously as an indicator for the supramolecular assembly of **PPC** aggregates in solution.

For β-sheet dominated polypeptides a negative band at $\lambda = 216$ nm and a positive band at $\lambda = 200$ nm are expected.[53,54] The computational results can explain these apparent differences between standard β-sheet spectra and the observed **PPC** spectrum. A CD spectrum $[\theta]_\lambda$ is the linear combination of the CD signals of the individual structural features $S_{\lambda i}$ with the coefficient F_i.[55] The competing P_{II} conformation seen in the molecular dynamics

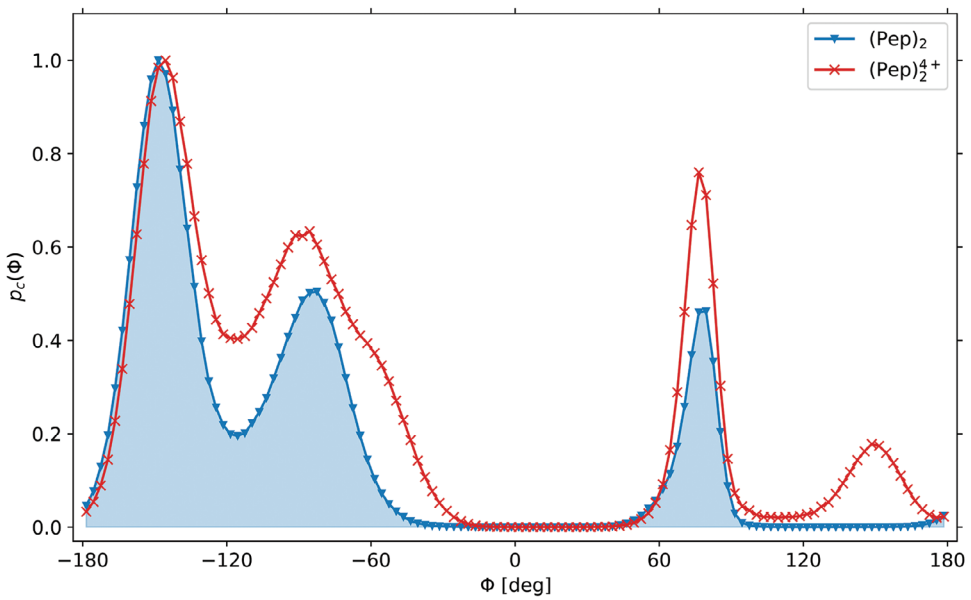

Figure 7. Contracted Ramachandran plots of Ac-FHFHFXG-OH dimers $(\mathbf{Pep})_2$ (blue) and the protonated counterpart $(\mathbf{Pep})_2^{4+}$ (red). The dominant structural feature is the β-sheet ($\Phi = (-150°)$) both in the neutral and charged states. Upon full protonation, the probability $p_c(\Phi)$ of the P_{II} ($\Phi = (-80°)$) and δ' ($\Phi = (80°)$) regions increase, proving a change in secondary structure in the charged state. Protonation of the side chains leads to dissociation of the polypeptide chains, and the two chains exhibit an increased unfolded conformation.

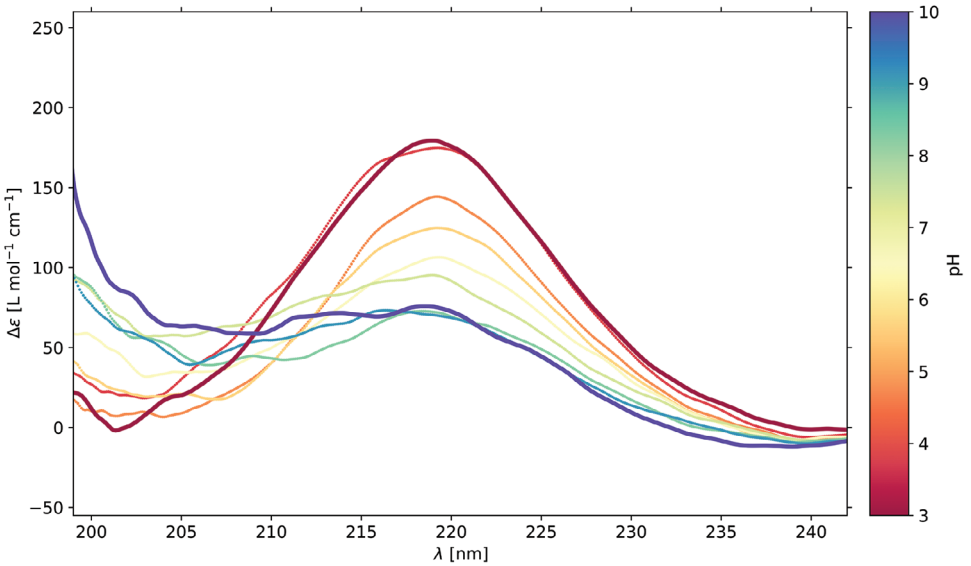

Figure 8. Circular dichroism spectrum of **PPC** at different pH values at room temperature. Upon increasing pH values the positive band at 220 nm decreases, while a positive plateau region between 200 and 210 nm emerges. The positive signal at 220 nm is characteristic for P_{II} secondary structures. At higher pH values aggregation and β-sheet is possible due to the deprotonation of the imidazolium side chains. The superposition of the P_{II} signal and β-sheet signal leads to a signal decrease at 220 nm. Data was smoothed for visualization purposes.

simulations of unfolded **Pep** can qualitatively account for the positive CD band at $\lambda = 200$ nm. P_{II} structures exhibit broad positive bands at $\lambda = 225$ nm and negative bands at $\lambda = 206$ nm significantly reducing the observed intensity of the β-sheet signals.[56] Considering that the observed signal at $\lambda = 220$ nm is positive, the P_{II} intensity of unfolded chains is dominant in the CD spectrum of **PPC**.

Since circular dichroism is a quantum mechanical effect, the molecular dynamics simulations presented here cannot predict any weighing coefficients F_i. They can only serve as a starting point for a more quantitative approach to fully predicting the CD spectrum. Nevertheless, the simulated structures of the Ac-FHFHFXG-OH fragment systems strongly suggest a new interpretation of the decreased signal at $\lambda = 220$ nm upon deprotonation and heating. The strongly decreased intensity of the band at $\lambda = 220$ nm from $\Delta\epsilon = 20\,\mathrm{L\,mol^{-1}cm^{-1}}$ (pH 3.0) to $\Delta\epsilon = 5\,\mathrm{L\,mol^{-1}cm^{-1}}$ (pH 10.3) can be explained by a dissociated state with unfolded chains exhibiting predominantly P_{II} conformations at low pH values. As described earlier, the fragment system shows a β-sheet dominated structure in the aggregated state

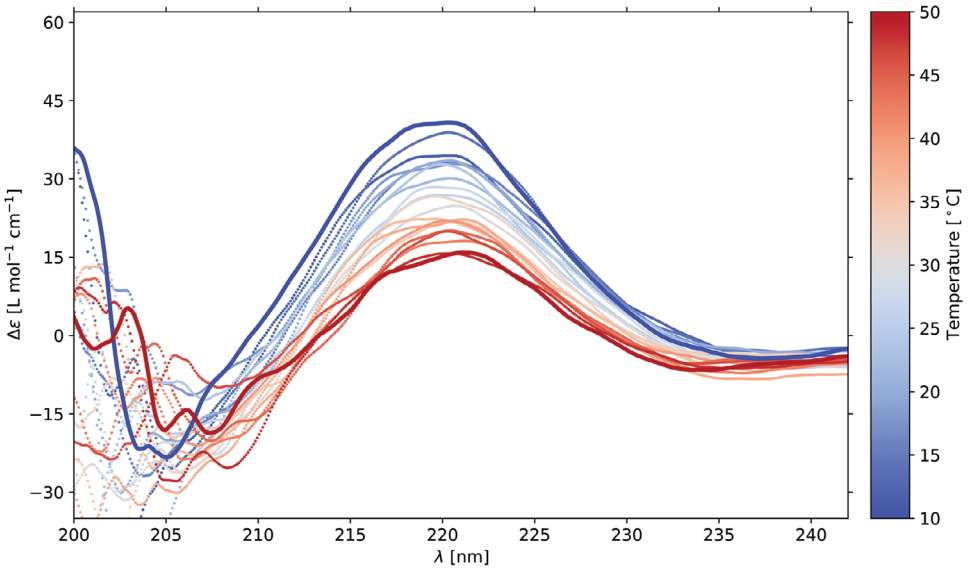

Figure 9. Circular dichroism spectrum of **PPC** at pH 7 at different temperatures. When temperature increases, the positive band at 220 nm decreases. The positive signal at 220 nm is characteristic for P_{II} secondary structures. The decrease of this signal can be explained by an increase in α-helix structures of unfolded chains upon temperature increase. Data was smoothed for visualization purposes.

and a decreased population of the P_{II} space, therefore lowering the relative intensity of the observed CD signal at $\lambda = 220$ nm. Consequently, this CD band at $\lambda = 220$ nm is a valid indicator for the supramolecular assembly of the **PPC** molecules, but it indicates a $P_{II} \rightarrow \beta$-sheet transition instead of the previously assumed random coil $\rightarrow \beta$-sheet transition. At higher pH values, the negative band between $\lambda = 200$ nm and $\lambda = 205$ nm becomes a plateau, which can also be explained by an increased contribution of the expected positive β-sheet signal at $\lambda = 200$ nm to the spectrum. Since the secondary structure of the unfolded chains was assumed to be in a random coil state, their contribution to the CD spectrum was not properly understood. This study proves that aMD simulations can unveil unexpected structures and, therefore, guide the interpretation of CD spectra.

When increasing the temperature at neutral pH values (pH 7.8), the CD band at $\lambda = 220$ nm decreases from $\Delta\epsilon = 8\ \mathrm{L\,mol^{-1}\,cm^{-1}}$ down to $\Delta\epsilon = 2.5\ \mathrm{L\,mol^{-1}\,cm^{-1}}$. The fact that this signal decrease is less pronounced compared to that upon changing the pH can be attributed to the conformational change of unfolded chains at higher temperatures. Unfolded chains show a decreased probability of adopting the P_{II} structure at higher temperatures, as has been seen in the single chain **Pep** simulations. As described above, this high-temperature-induced conformational change leads to an increase in α-helical structures. These α-helical structures exhibit an intense negative band at $\lambda = 222$ nm in CD spectra, explaining the apparent decrease of the observed CD signal at $\lambda = 220$ nm with increasing temperature.[15]

Even in the fully protonated state (Figure 8) and at high temperatures (Figure 9) a residual positive signal at $\lambda = 220$ nm is observed. We attribute this to intramolecular $\pi - \pi$ stacking between the aromatic phenylalanine rings as reported previously.[57] We do appreciate that due to the spectral overlap of the P_{II} specific CD signatures and the CD band related to $\pi - \pi$ stacking, it is not possible to fully assign the contribution from each of those interactions to the CD spectra. However, because of the pronounced pH dependency of the observed signal at $\lambda = 220$ nm we conclude that the dominant contribution to the CD spectrum at acidic pH values relates to the P_{II} conformation, which decreases caused by a change in the secondary structure and aggregation of the molecules.

4. Conclusion and Outlook

Knowledge of the kinetic pathways of polypeptide folding and unfolding dynamics is crucial for understanding possible mechanisms of the self-assembly, the resulting material properties, and the potential biological activity of these molecules. The present study significantly advances our understanding of the structural dynamics and assembly mechanism of ABA-type polymer peptide conjugates. Our comprehensive computational analyses, employing atomistic molecular dynamics simulations, have allowed us to identify the anti-parallel β-sheet as the dominant secondary structure of Ac-FHFHFXG-PEO_n-GXFHFHF-Ac aggregates in solution while highlighting their sensitivity to temperature and pH changes. Even though aMD simulations cannot predict the circular dichroism spectra of polypeptides directly, the calculated secondary structures and transient intermediates can serve as a powerful guide to interpreting complex CD spectra. Here, we identified a β-sheet to P_{II} transition upon full protonation of the polypeptide, which coincided with experimental circular dichroism data of the polymer peptide conjugate, challenging the previous interpretation of these CD spectra.

This work could be extended in several directions. Refinements of the method could further strengthen the analysis and provide additional insights: The Ramachandran analysis is error-prone to statistical fluctuations when only a few amino acids contribute to the dihedral angle distribution.[58] More sophisticated sampling and clustering approaches could alleviate this problem. Experimentally, the predicted geometry could be confirmed using experimental techniques like 2D-NMR or scattering methods.[59,60]

While using a smaller fragment system was successful in qualitatively predicting the CD spectrum, interactions between the PEO chains and the peptides and higher-order interactions between aggregates larger than dimers were ignored. In particular, the interplay of PEO chain conformations and structure formation of peptides, and the potentially stabilizing effect of PEO chains, will be an interesting topic for future work. When looking at even larger systems containing several polymer peptide conjugates, aMD simulations become increasingly challenging due to their high computational costs. Here, coarse-grained simulations provide a promising alternative that could be used to study aggregation pathways on larger scales. It will also be interesting to use titratable models instead of fixed protonation states.[61]

The general methodology presented here is not limited to our specific system but can be applied to various polymer peptide conjugates. This research thus lays a foundational groundwork for future investigations. It calls for more comprehensive studies involving larger aggregates and refined models, paving the way for deeper understanding and innovative applications in polymer peptide conjugate self-assembly specifically, and synthetic biomimetic polymer structures in general.

Supporting Information

Supporting Information is available from the Wiley Online Library or from the author.

Acknowledgements

Funding from the DFG (Deutsche Forschungsgemeinschaft) was acknowledged. P.B. and F.S. were members and M.S. was an associate Ph.D. student of the GRK 2516 (Project No. 405552959). M.S. was the recipient of a doctoral fellowship from the Max Planck Graduate Center with the Johannes Gutenberg University Mainz (MPGC). The authors gratefully acknowledged the computing time granted on the supercomputer MOGON II at Johannes Gutenberg University Mainz as part of NHR South-West (nhrsw.de).

Open access funding enabled and organized by Projekt DEAL.

Conflict of Interest

The authors declare no conflict of interest.

Data Availability Statement

The data that support the findings of this study are available from the corresponding author upon reasonable request.

Keywords

circular dichroism, molecular dynamics simulation, peptide-conjugation, stimulus-responsive, supramolecular self-assembly

Received: March 14, 2024
Revised: June 16, 2024
Published online: July 8, 2024

[1] M. A. Gauthier, H.-A. Klok, *Chem. Commun.* **2008**, *1*, 2591.
[2] I. W. Hamley, *Biomacromolecules* **2014**, *15*, 1543.
[3] L. A. Canalle, D. W. P. M. Löwik, J. C. M. v. Hest, *Chem. Soc. Rev.* **2009**, *39*, 329.
[4] R. Behrendt, P. White, J. Offer, *J. Pept. Sci.* **2016**, *22*, 4.
[5] C. A. Stevens, K. Kaur, H.-A. Klok, *Adv. Drug Delivery Rev.* **2021**, *174*, 447.
[6] P. A. Taylor, A. Jayaraman, *Annu. Rev. Chem. Biomol. Eng.* **2020**, *11*, 257.
[7] S. Kmiecik, D. Gront, M. Kolinski, L. Wieteska, A. E. Dawid, A. Kolinski, *Chem. Rev.* **2016**, *116*, 7898.
[8] D. J. Beltran-Villegas, D. Intriago, K. H. C. Kim, N. Behabtu, J. D. Londono, A. Jayaraman, *Soft Matter* **2019**, *15*, 4669.
[9] H. Lee, *Pharmaceutics* **2020**, *12*, 533.
[10] J. Subbotina, I. Rouse, V. Lobaskin, *Nanoscale* **2023**, *15*, 13371.
[11] E. Hamed, D. Ma, S. Keten, *BioNanoScience* **2015**, *5*, 140.
[12] E. Hamed, T. Xu, S. Keten, *Biomacromolecules* **2013**, *14*, 4053.
[13] A. Jain, H. S. Ashbaugh, *Biomacromolecules* **2011**, *12*, 2729.
[14] S. M. Kelly, N. C. Price, *Biochim. Biophys. Acta, Protein Struct. Mol. Enzymol.* **1997**, *1338*, 161.
[15] D. M. Rogers, S. B. Jasim, N. T. Dyer, F. Auvray, M. Réfrégiers, J. D. Hirst, *Chem* **2019**, *5*, 2751.
[16] N. J. Greenfield, *Methods Enzymol.* **2004**, *383*, 282.
[17] V. Hall, A. Nash, E. Hines, A. Rodger, *J. Comput. Chem.* **2013**, *34*, 2774.
[18] L. Zhao, J. Zhang, Y. Zhang, S. Ye, G. Zhang, X. Chen, B. Jiang, J. Jiang, *JACS Au* **2021**, *1*, 2377.
[19] N. Sreerama, R. W. Woody, *Methods Enzymol.* **2004**, *383*, 318.
[20] E. D. Drew, R. W. Janes, *Nucleic Acids Res.* **2020**, *48*, W17.
[21] R. Otter, N. A. Henke, C. Berac, T. Bauer, M. Barz, S. Seiffert, P. Besenius, *Macromol. Rapid Commun.* **2018**, *39*, 1800459.
[22] C. Pascouau, M. Schweitzer, P. Besenius, *Biomacromolecules* **2024**, *25*, 2659.
[23] J. M. Briggs, T. Matsui, W. L. Jorgensen, *J. Comput. Chem.* **1990**, *11*, 958.
[24] M. J. Robertson, Y. Qian, M. C. Robinson, J. Tirado-Rives, W. L. Jorgensen, *J. Chem. Theory Comput.* **2019**, *15*, 2734.
[25] Y. Sakae, Y. Okamoto, *Mol. Simul.* **2010**, *36*, 1148.
[26] M. J. Robertson, J. Tirado-Rives, W. L. Jorgensen, *J. Chem. Theory Comput.* **2015**, *11*, 3499.
[27] G. A. Kaminski, R. A. Friesner, J. Tirado-Rives, W. L. Jorgensen, *J. Phys. Chem. B* **2001**, *105*, 6474.
[28] O. Guvench, A. D. MacKerell, *Methods Mol. Biol.* **2008**, *443*, 63.
[29] W. L. Jorgensen, J. Chandrasekhar, J. D. Madura, R. W. Impey, M. L. Klein, *J. Chem. Phys.* **1983**, *79*, 926.
[30] J. Henriques, M. Skepoö, *J. Chem. Theory Comput.* **2016**, *12*, 3407.
[31] W. L. Jorgensen, *J. Chem. Phys.* **1982**, *77*, 4156.
[32] L. S. Dodda, I. Cabeza de Vaca, J. Tirado-Rives, W. L. Jorgensen, *Nucleic Acids Res.* **2017**, *45*, W331.
[33] W. L. Jorgensen, J. Tirado-Rives, *Proc. Natl. Acad. Sci.* **2005**, *102*, 6665.
[34] W. L. Jorgensen, J. Tirado-Rives, *J. Am. Chem. Soc.* **1988**, *110*, 1657.
[35] L. S. Dodda, J. Z. Vilseck, J. Tirado-Rives, W. L. Jorgensen, *J. Phys. Chem. B* **2017**, *121*, 3864.
[36] T. A. Halgren, *J. Comput. Chem.* **1996**, *17*, 490.
[37] M. L. Obenauer, K. N. Spauszus, P. Besenius, F. Schmid, *J. Open Source Softw.* **2024**, *9*, 6293.
[38] J. Lemkul, *Living J. Comput. Mol. Sci.* **2019**, *1*, 1.
[39] G. Bussi, D. Donadio, M. Parrinello, *J. Chem. Phys.* **2007**, *126*, 014101.
[40] U. Essmann, L. Perera, M. L. Berkowitz, T. Darden, H. Lee, L. G. Pedersen, *J. Chem. Phys.* **1995**, *103*, 8577.
[41] S. Pronk, S. Páll, R. Schulz, P. Larsson, P. Bjelkmar, R. Apostolov, M. R. Shirts, J. C. Smith, P. M. Kasson, D. van der Spoel, B. Hess, E. Lindahl, *Bioinformatics* **2013**, *29*, 845.
[42] S. Páll, M. J. Abraham, C. Kutzner, B. Hess, E. Lindahl, in *Solving Software Challenges for Exascale*, (Eds.: S. Markidis, E. Laure), Springer International Publishing, Cham **2015**, pp. 3–27.
[43] M. Parrinello, A. Rahman, *J. Appl. Phys.* **1981**, *52*, 7182.
[44] B. Hess, H. Bekker, H. J. C. Berendsen, J. G. E. M. Fraaije, *J. Comput. Chem.* **1997**, *18*, 1463.
[45] J. Lemkul, *Living J. Comput. Mol. Sci.* **2019**, *1*, 1.
[46] R. Gowers, M. Linke, J. Barnoud, T. Reddy, M. Melo, S. Seyler, J. Domański, D. Dotson, S. Buchoux, I. Kenney, O. Beckstein, *Proceedings of the 15th Python in Science Conference*, United States **2016**, pp. 98–105.
[47] N. Michaud-Agrawal, E. J. Denning, T. B. Woolf, O. Beckstein, *J. Comput. Chem.* **2011**, *32*, 2319.
[48] C. R. Harris, K. J. Millman, S. J. v. d. Walt, R. Gommers, P. Virtanen, D. Cournapeau, E. Wieser, J. Taylor, S. Berg, N. J. Smith, R. Kern, M. Picus, S. Hoyer, M. H. v. Kerkwijk, M. Brett, A. Haldane, J. F. d. Río, M. Wiebe, P. Peterson, P. Gérard-Marchant, K. Sheppard, T. Reddy, W. Weckesser, H. Abbasi, C. Gohlke, T. E. Oliphant, *Nature* **2020**, *585*, 357.
[49] S. A. Hollingsworth, P. A. Karplus, *Biomol. Concepts* **2010**, *1*, 271.
[50] K. B. O. Chatzi, D. Gatos, G. Stavropoulos, *Int. J. Pept. Protein Res.* **1991**, *37*, 513.
[51] N. C. Fitzkee, P. J. Fleming, H. Gong, N. Panasik, T. O. Street, G. D. Rose, *Trends Biochem. Sci.* **2005**, *30*, 73.
[52] Z. Shi, R. W. Woody, N. R. Kallenbach, *Adv. Protein Chem.* **2002**, *62*, 163.
[53] S. M. Kelly, N. C. Price, *Biochim. Biophys. Acta, Protein Struct. Mol. Enzymol.* **1997**, *1338*, 161.
[54] M. C. Manning, M. Illangasekare, R. W. Woody, *Biophys. Chem.* **1988**, *31*, 77.
[55] S. Zhu, M. Sun, *Appl. Spectrosc. Rev.* **2021**, *56*, 553.
[56] R. W. Woody, *J. Am. Chem. Soc.* **2009**, *131*, 8234.
[57] N. Amdursky, M. M. Stevens, *ChemPhysChem* **2015**, *16*, 2768.
[58] L. J. Smith, K. M. Fiebig, H. Schwalbe, C. M. Dobson, *Fold. Des.* **1996**, *1*, R95.
[59] M. Kjaergaard, F. M. Poulsen, *J. Biomol. NMR* **2011**, *50*, 157.
[60] U. B. Gawas, V. K. Mandrekar, M. S. Majik, in *Advances in Biological Science Research* (Eds: S. N. Meena, M. M. Naik), Elsevier, **2019**, pp. 69–84.
[61] F. Grünewald, P. C. T. Souza, H. Abdizadeh, J. Barnoud, A. H. d. Vries, S. J. Marrink, *J. Chem. Phys.* **2020**, *153*, 024118.

